electronics

Article

Adaptive Load Balancing for Dual-Mode Communication Networks in the Power Internet of Things

Kunpeng Xu [1], Zheng Li [1], Yunyi Yan [2], Hongguang Dai [1], Xianhui Wang [1,*], Jinlei Chen [1] and Zesong Fei [2]

[1] Beijing Smart Chip Microelectronic Co., Ltd., Beijing 102200, China; xukunpeng@sgchip.sgcc.com.cn (K.X.); lizheng1@sgchip.sgcc.com.cn (Z.L.); daihongguang@sgchip.sgcc.com.cn (H.D.); chenjinlei@sgchip.sgcc.com.cn (J.C.)
[2] School of Information and Electronics, Beijing Institute of Technology, Beijing 100081, China; yanyunyi@bit.edu.cn (Y.Y.); feizesong@bit.edu.cn (Z.F.)
* Correspondence: wangxianhui1@sgchip.sgcc.com.cn

Abstract: As an important part of the power Internet of Things, the dual-mode communication network that combines the high-speed power line carrier (HPLC) mode and high-speed radio frequency (HRF) mode is one of the hot directions in current research. Since non-uniform transmission demands for power consumption information can lead to link congestion among nodes, improving the network load-balancing performance becomes a critical issue. Therefore, this paper proposes a load-balancing routing algorithm for dual-mode communication networks, which is achieved in dual-mode communication networks by adding alternate paths and proxy coordinator (PCO) node election mechanism. Simulation results show that the proposed algorithm achieves the load-balanced distribution of power consumption information transmission. The proposed scheme reduces the delay and packet loss rate, as well as improving the throughput of dual-mode communication compared to existing routing algorithms.

Keywords: dual-mode communication; routing algorithm; load balancing; PCO node election

Citation: Xu, K.; Li, Z.; Yan, Y.; Dai, H.; Wang, X.; Chen, J.; Fei, Z. Adaptive Load Balancing for Dual-Mode Communication Networks in the Power Internet of Things. *Electronics* **2023**, *12*, 4366. https://doi.org/10.3390/electronics12204366

Academic Editors: Arne Bröring and Djuradj Budimir

Received: 7 September 2023
Revised: 13 October 2023
Accepted: 19 October 2023
Published: 21 October 2023

1. Introduction

With the rapid development of communication hardware and software technology, smart grids can realize real-time monitoring, control, and management of the power system [1]. Smart grids can collect a large amount of data and utilize smart infrastructure for advanced management, which do their best to achieve the goals of improving energy efficiency, balancing supply and demand, controlling emissions, reducing operating costs, and maximizing utility [2–4]. High-speed power line carrier (HPLC) communication and High-speed radio frequency (HRF) are two common modes of communication in the power Internet of Things. The HPLC network is considered a convenient and economical solution for the smart grid because HPLC utilizes the wire and power outlet infrastructure that has already been constructed without rewiring [5]. In addition, relevant reports indicate that the data rate of HPLC can be up to hundreds of megabits per second or even gigabits per second, which is sufficient to support most of the services in the smart grid [6]. However, there are some challenges such as high volatility of electrical loads, strong time-varying characteristics of line impedance, severe noise interference on long-distance lines, and blockage of distribution transformers affecting power line carrier (PLC) signal transmission [7]. In addition, HPLC communication makes it difficult to adjust the routing flexibly in the face of congestion due to the reliance on existing grid lines, which leads to a serious deterioration of system performance. On the other hand, HRF communication is self-organizing in the formation of routing networks by adjusting their roles in the network because they do not need to be wired in advance [8]. However, the quality of HRF communication in different environments is susceptible to interference, especially when encountering obstacles with severe signal attenuation [9]. In addition, nodes in HRF networks may be placed in hard-to-reach locations, making it impossible to charge their limited batteries on time. The problem of energy consumption becomes one of the key challenges in HRF networks [10].

For complex scenarios such as high-density services, high urbanization, high-rise buildings, and underground floors [11], smart grids require better transmission rates, wider connectivity, and higher robustness [12]. To solve the problems that arise from the use of single-mode HPLC or HRF in smart grids, several studies have combined HPLC mode with HRF mode to improve the reliability of existing connections and the ability to transmit data in recent years [13].

As dual-mode communication technology continues to be updated, more and more users are choosing to use dual-mode communication, which brings about some challenging research issues. Numerous studies have shown that since areas with dense users generate larger communication demand than areas with sparse users, this can result in a very uneven distribution of traffic throughout the network. Some nodes have taken up a large number of communication tasks, leading to a drop in the available bandwidth for transmitting and an increase in the occupancy of the buffer zone, and serious congestion has occurred. On the other hand, some nodes are not required to undertake a large number of communication tasks, leading to low utilization rate [14]. If the traffic load in the network continuously passes through congested nodes, it will inevitably lead to deterioration of network delay, throughput, and packet loss.

In this paper, we study the load-balancing mechanism for dual-mode communication networks and design a routing algorithm to improve performance. As shown in Figure 1, our contributions are summarized below.

- We design a complete routing and networking process for dual-mode communication. Firstly, utilizing the improved mean shift algorithm, the station (STA) nodes are divided into different clusters centered around proxy coordinator (PCO) [15] nodes. The meter information collected by the STAs is forwarded through PCOs to reach the central coordinator (CCO) [15]. The proposed process adopts different transmission strategies based on congestion conditions. When only a few PCO nodes experience congestion, the alternate path is used to complete the transmission of meter information. When a significant number of PCO nodes encounter congestion, the PCO node election mechanism is employed to ensure the reliability of the link during the re-networking process. The proposed process gives a good solution for the traffic balancing problem of dual-mode communication.
- We propose adding alternate paths between PCO nodes and STA nodes in the traditional tree network to enhance the network's ability to adapt to congestion. When there are fewer PCO nodes in the congested state, the alternate path can transfer some of the traffic from the congested region to the uncongested region. Simulation results show that lower delay and packet loss rates are obtained and throughput is improved compared to the traditional scheme.
- A load-balancing routing algorithm is proposed, based on the PCO node election mechanism and the shortest hop path algorithm. The PCO nodes with low buffer occupancy and high available transmit bandwidth are selected to replace the PCO nodes in a congested state during the re-networking process. Simulation results show that the proposed method not only effectively alleviates congestion when more PCO nodes are in a congested state, but also achieves lower delay, packet loss, and improved throughput compared to the traditional scheme.

The rest of the paper is organized as follows: Section 2 describes previous research. Section 3 describes our system model and the definition of network performance parameters. Section 4 describes the network establishment process. In Section 5, the sending rate and cache occupancy are taken into account and then a load-balancing routing algorithm based on the PCO node election mechanism is introduced. Simulation results are shown and discussed in Section 6. Section 7 summarizes and discusses the simulation results. Finally, the paper is concluded in Section 8.

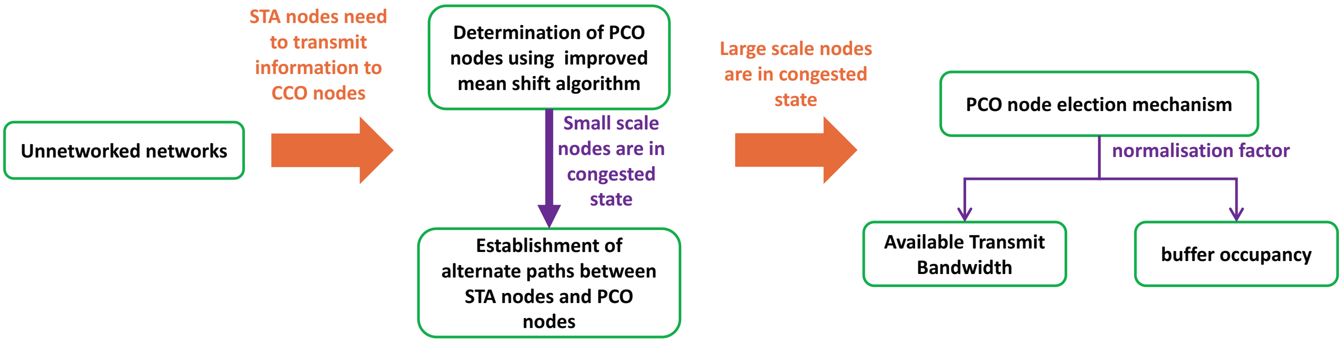

Figure 1. Graphic abstracts that present the main steps of the proposed scheme.

2. Related Work

Many studies have been conducted to solve the balancing problem by optimizing the cluster heads as follows. Several methods based on cluster head (CH) election have been proposed to distribute the load of CH among the nodes in the network. Low energy adaptive clustering hierarchy (LEACH) is a classical algorithm that randomly selects the CH in each round and subsequently the CH communicates with each member node in the cluster to collect the sensed data [16]. The probability of a node becoming a cluster head is based on a pre-set ratio of cluster heads to all nodes and the number of times it has become a cluster head. The nodes within the cluster then access the cluster head with the lowest communication load. The LEACH algorithm exhibits considerable potential for refinement due to the inherent stochasticity associated with the selection of CHs, prompting a plethora of scholars to conduct extensive and meaningful research endeavors to explore and augment its efficacy. The optimization of cluster head selection in the network was further achieved by considering the initial energy, residual energy, optimal value of the number of CHs, the distance between nodes, etc. during the rotation of cluster nodes [17–20]. However, failing to account for the receiving capacity of the cluster head can lead to suboptimal network performance. Adil et al. proposed a Dynamic Cluster Based Static Routing Protocol (DCBSRP) combined with Ad hoc On-demand Distance Vector (AODV) routing protocol and LEACH protocol for network routing [21]. After the initial determination of cluster heads based on LEACH protocol, the node that receives the most routing replies (RREPs) is selected as the next round of CH nodes. Once the CH node is confirmed, the DCBSRP routing protocol binds all common nodes to the specified CH node by applying a static routing configuration. Some nodes are distributed in more remote locations which causes single-hop communication to be not always a perfect solution. Further, considering the cluster head election problem in multi-hop communication can suggest a better solution for complex node distribution [22–29]. In real-world application scenarios, network nodes exhibit significant heterogeneity in their capabilities, configurations, and behaviors [30]. To address this heterogeneity, the cluster head with both maximum residual energy and maximum initial energy is elected in each round [31–35].

The above approach solves the energy balancing problem well by using cluster head rotation. However, energy balancing does not take into account the congestion that can occur in dual-mode communication networks. Extending the network lifetime through energy equalization does not necessarily improve the performance of the transmission, and the degradation of the communication capability of the PCO nodes in a congested state continues to affect the operation of other types of nodes. The initial research considered the classical Dijkstra algorithm to identify the path with the shortest distance from the source node to the destination node [36]. The strategy using the greedy algorithm starts from the source node and gradually searches outwards until it extends to the destination node. Some studies have adopted the method of obtaining link congestion information through a status notification mechanism and directing traffic to less congested links based on this link congestion information [37–40]. In the method proposed by Taleb et al., the node that is about to experience congestion requires neighboring nodes to reduce the data forwarding rate [37,38]. The number of nodes in the congested state within the network tends to increase gradually with the rise in the volume of services, and considering only local re-planning of paths will not give a good solution. A set of traffic lights is used to indicate the congested state of the current node and the next node in the traffic-light-based intelligent routing strategy (TLR) proposed by Song et al. When a packet travels to its destination along a pre-calculated route, the route can be dynamically adjusted according to the real-time color of the traffic lights at each intermediate node. At the same time, neighboring nodes search for the path where traffic lights show less congestion and transmit part of the data from the congested node on that path [39]. Although the above algorithms can balance the network congestion to a certain extent, they suffer from the problem of local optimality and may not be able to balance the congestion of the whole network. To achieve better global traffic balancing, the algorithm proposed by Dong et al. utilizes more global link congestion information, an effective congestion avoidance mechanism, and a state notification mechanism that combines active discovery and automatic detection [40]. However, the state notification mechanism makes the network take a longer time to get information about the nodes that are in a congested state. A simplified energy-balanced alternative-aware routing algorithm (SEAR) was proposed by MU et al. [41]. SEAR repairs links faster by adding a link field to the routing table that determines whether a link is broken due to congestion. Meanwhile, when the link is broken, the source node is able to repair the communication capability of the link between the transmitting nodes without the need for the source node to re-initiate the route request process, which reduces the data transmission delay and network overhead. As long as a certain size of non-congested area exists in the whole network, re-routing ensures the reliability of the network. However, the above mechanisms will not give a good solution for uncongested regions that do not reach a specific size within the network. In addition, to the best of our knowledge, previous studies on dual-mode communication networks have not considered the fact that traffic loads are accumulating on the proxy coordinator (PCO) nodes that act as cluster heads leading to the occurrence of congestion. During transmission, the situation where a large number of PCO nodes become congested still cannot be handled.

3. System Model

3.1. Node Model

In this section, we present a scenario of collecting electricity consumption information using a dual-mode communication network as a component of the smart grid.

The nodes in dual-mode communication are spatially static and uniformly distributed. They are primarily used for monitoring and transmitting electricity consumption information within a specific area. In this paper, we considered the heterogeneity of nodes in the network, which have varying available transmit bandwidths and buffer sizes. There are three types of nodes in the dual-mode communication network: the central coordinator (CCO), the PCO, and the station (STA). The relationship between the three nodes in the dual-mode communication is shown in Figure 2. The definitions and specific functions of the three types of nodes are introduced as follows.

- STA: The STA nodes are devices used to measure and monitor power consumption in a dual-mode communication network. In the meter reading scenario, STA nodes can communicate with CCO nodes through a defined path for informatization and intelligence of the power grid. The STA nodes are spatially deployed randomly and periodically send the electricity consumption information from the detection area to the CCO nodes.
- PCO: The PCO node serves as the relay node in the dual-mode communication network. Its main responsibility is to collect and aggregate data from STA nodes within a specific region. The PCO node then transmits these data to other nodes or higher-level nodes in the network, following the path determined by the CCO node. This process enables the aggregation and forwarding of data.

- CCO: The CCO node is a central control node of the dual-mode communication network and is responsible for coordinating and managing the routing network of the entire network. The CCO nodes receive electricity consumption information from STA nodes in each region, and realize real-time monitoring, remote control, and intelligent management of electrical energy data. The main functions of the CCO node are the management of node link resources in the dual-mode communication network, processing routing requests in the network, performing load-balancing algorithms to optimize traffic distribution, and ensuring the efficient operation of the network. The CCO node is fixed and assumed to have sufficient hardware equipment with nearly unlimited transmit bandwidth and buffer size compared with the STA and PCO nodes.

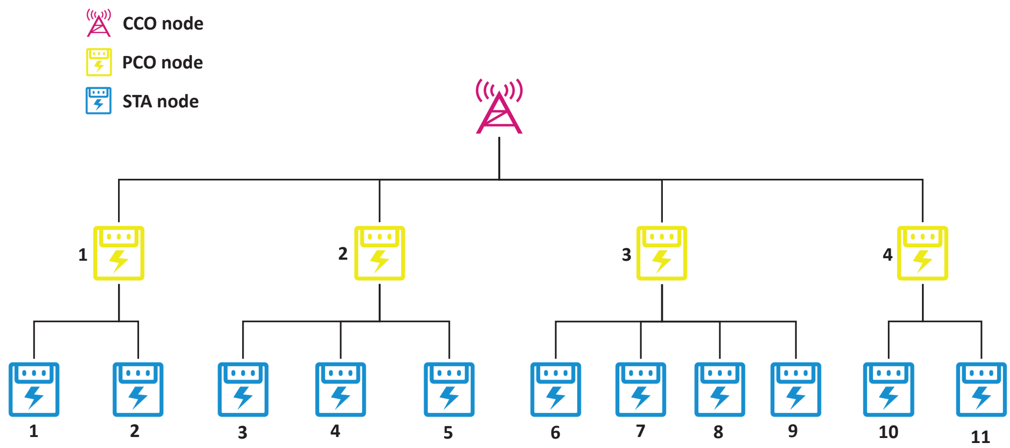

Figure 2. Layered structure diagram.

3.2. Topology

To reduce the complexity of the communication network routing process, improve the efficiency of the communication network, and reduce the interference between different nodes, the mean shift algorithm is used to divide the communication network into three layers as shown in Figure 2 [42]. The mean shift algorithm determines the PCO nodes and the STA nodes that access the corresponding PCO nodes based on the node density. The advantage of the mean shift algorithm over the k-mean algorithm [43], which also achieves clustering, is that it does not need to predetermine the number of PCO nodes. It can adaptively determine the number of PCO nodes based on the radius of convergence and the node distribution of the network. Nodes between adjacent layers in the network can communicate directly, but nodes between different layers that are not adjacent need to be forwarded to the destination node through an intermediate layer node as a relay node. For example, in Figure 2 STA node No. 4 cannot send the electricity consumption information to the CCO node by single-hop, so its information needs to be forwarded to the CCO node through PCO node No. 2, which acts as a relay node.

Suppose a dual-mode communication network is used for meter information reading; the topology of the network can be represented by graph $G = (Node, Link)$, where $Node = \{Node_i | 0 \leq i \leq N-1\}$ denotes the communication node set in the dual-mode communication network and $Link = \{Link_{i,j} | 0 \leq i \leq N-1, 0 \leq j \leq N-1, i \neq j\}$ denotes the communication link between the dual-mode node i and node j.

3.3. Key Performance Metrics

3.3.1. Delay

A large amount of power consumption information needs to be collected in dual-mode communication, but the ability of nodes to receive, process, and send data, as well as the capacity of the link to transmit data, is limited, which leads to a delay in sending the power consumption information from the source node to the destination node.

The delay of link $Link_{i,j}$ can be expressed as [40]:

$$Delay_{i,j} = T_{queue}^{i,j} + T_{prop}^{i,j}, \tag{1}$$

where $T_{queue}^{i,j}$ represents the queuing delay of link $Link_{i,j}$ and $T_{prop}^{i,j}$ represents the propagation delay of link $Link_{i,j}$. The propagation delay is defined as follows:

$$T_{prop}^{i,j} = \frac{D_{i,j}}{c}, \tag{2}$$

where $D_{i,j}$ represents the physical length of the link $Link_{i,j}$, and c represents the speed of light, which is taken as 3×10^8 m/s. Since the values of $T_{prop}^{i,j}$ and $T_{queue}^{i,j}$ have a large difference in order of magnitude, $T_{prop}^{i,j}$ can be ignored in the delay calculation for the link $Link_{i,j}$.

Therefore, the delay of link $Link_{i,j}$ in a dual-mode communication network can be can be simplified to:

$$Delay_{i,j} = T_{queue}^{i,j}. \tag{3}$$

To obtain a specific expression for the queuing delay, it is necessary to first define the length of the packet queue as follows:

$$Queue_i^{t+1} = \min\{[Queue_i^t + N_{in,i}^t - N_{out,i}^t], Buffersize_i\}, \tag{4}$$

where $Queue_i^t$ represents the queue length that is occupied by node i at the period t of the dual-mode communication cycle. $N_{in,i}^t$ and $N_{out,i}^t$ are the amount of input and output data for node i at period $t+1$ in dual-mode communication cycle, respectively, and $Buffersize_i$ is the size of the entire buffer for node i. $N_{out,i}^t$ is defined as follows:

$$N_{out,i}^t = B_{\max,i}^t \cdot B_{available,i}^t \cdot T_{queue}^{i,j}, \tag{5}$$

where $B_{\max,i}^t$ is the maximum communication bandwidth for node i at the period t of the dual-mode communication cycle and $B_{occupancy,i}^t$ is the available bandwidth factor of node i at the period t. The value of the available bandwidth factor $B_{occupancy,i}^t$ is influenced by different hardware structures and congestion levels.

The queuing delay is defined by Equation (5) as follows:

$$T_{queue}^{i,j} = \frac{N_{out,i}^t}{B_{\max,i}^t \cdot B_{occupancy,i}^t}. \tag{6}$$

Let K be the number of feasible communication paths from the source node s to the destination node d; $Path_{s,d}^k$ denotes the $k\,th$ path in the set of feasible communication paths.

The expression for the total time delay along path $Path_{s,d}^k$ from source node s to destination node d is further given by Equation (7) as follows:

$$Delay_{s,d}^{Path_{s,d}^k} = \sum_{\forall link_{i,j} \in Path_{s,d}^k} Delay_{i,j}^{link_{i,j}}, \tag{7}$$

where $Delay_{i,j}^{link_{i,j}}$ is the time delay when the packet is transmitted on link $link_{i,j}$, which is a segment on the path $Path_{s,d}^k$ from node s to node d.

3.3.2. Packet Loss Rate

In dual-mode communication, nodes sometimes receive a large amount of power consumption information data, and the amount of data exceeds the node's ability to process the data, which will cause the occupied queue in the buffer to grow longer and longer. When the occupied queue length exceeds the maximum length that can be stored in the buffer, a serious load-shedding phenomenon occurs, and the packet loss rate increases rapidly.

The packet loss rate for node i at period $t+1$ in dual-lode communication is defined as follows [44]:

$$packetloss\_number_i^{t+1} = Queue_i^t + N_{in,i}^t - N_{out,i}^t - Buffersize_i, \tag{8}$$

where $Queue_i^t$ represents the queue length that is occupied by node i at the period t of the dual-mode communication cycle. $N_{in,i}^t$ and $N_{out,i}^t$ are the amount of input and output data for node i at period $t+1$ in dual-mode communication cycle, respectively, and $Buffersize_i$ is the size of the entire buffer for node i.

We use the packet loss rate to indicate the number of packets that are lost in the process compared to the total number of packets that are sent during transmission.

The definition of packet loss rate between node i and node j is given by Equation (8):

$$packetloss\_rate_{i,j} = \frac{packetloss\_number_i^{t+1}}{Queue_i^t + N_{in,i}^t - N_{out,i}^t}. \tag{9}$$

The total packet loss rate of the kth path in the path set from the source node to the destination node is given as follows:

$$packetloss\_rate_{s,d}^{Path_{s,d}^k} = 1 - \prod_{link_{i,j} \in Path_{s,d}^k} \left(1 - packetloss\_rate_{i,j}^{link_{i,j}}\right), \tag{10}$$

where $packetloss\_rate_{i,j}^{link_{i,j}}$ is the packet loss rate when the packet is transmitted on link $link_{i,j}$, which is a segment on the path $Path_{s,d}$ from node s to node d.

3.3.3. Throughput

Throughput is one of the important metrics to evaluate network performance and data transmission efficiency in dual-mode communication network routing. The throughput is the amount of data successfully transmitted from the source node to the destination node per unit time.

According to (5), (7), and (10), the throughput along path $Path_{s,d}^k$ from the source node s to the destination node d is defined as follows:

$$Throughput_{s,d}^{Path_{s,d}^k} = \frac{B_{\max,s} \cdot B_{available,s} \cdot packetloss\_rate_{s,d}^{Path_{s,d}^k}}{Delay_{s,d}^{Path_{s,d}^k}}, \tag{11}$$

where $B_{\max,s}$ is the maximum communication bandwidth for source node s during a dual-mode communication cycle and $B_{available,s}$ is the available bandwidth factor of node s.

3.3.4. Flow

Flow represents the data stored in the buffer area that need to be transmitted in a dual-mode communication network during a specific period, which can be used to evaluate the level of congestion on a link.

The flow for node i at period $t+1$ in dual-mode communication by equation is defined as follows:

$$Flow_i^{t+1} = Queue_i^t + N_{in,i}^t - N_{out,i}^t, \tag{12}$$

where $Queue_i^t$ represents the queue length that is occupied by node i at the period t of the dual-mode communication cycle. $N_{in,i}^t$ and $N_{out,i}^t$ are the amount of input and output data for node i at period $t+1$ in the dual-mode communication cycle, respectively.

3.3.5. Congestion

We use $congestion\_state_i^t$ to denote the congestion status of node i at period t. The definition of $congestion\_state_i^t$ is given as follows:

$$congestion\_state_i^t = \begin{cases} 0 & \text{If node i is congested} \\ 1 & \text{If node i is normal} \end{cases}. \tag{13}$$

$congestion\_state_i^t$ is stored as a binary number within each STA and PCO node, and the STA and PCO nodes periodically transmit the value of a to the CCO node. When the value of $congestion\_state_i^t$ is 1, it means that node i is congested at period t, and when the value of $congestion\_state_i^t$ is 0, it means that node i at period t is not congested.

We define occupancy of the buffer as follows:

$$Quene_{occupancy,i}^t = \frac{Quene_i^t}{Buffersize_{i,t}}. \tag{14}$$

If the buffer queue length increases to be larger than the capacity of the buffer, the node drops the excess packets during the communication cycle. To avoid congestion, we define the node as being in a congested state when the length of the queue in the buffer of the node exceeds the capacity of the buffer, which means that the occupancy rate of the buffer exceeds 1 for node i at period t.

In addition, if the sending rate of a node is too slow, this will increase the time for the node to process the electricity consumption information in dual-mode communication, resulting in data traffic being blocked at that node for a long period. Let B_available denote the available sending bandwidth of node i at period t. The expression for a is given as follows:

$$B\_\text{available}_i^t = B_{\max,i}^t \cdot B_{occupancy,i}^t. \tag{15}$$

We define the available sending bandwidth threshold as $B\_\text{available}_{th,i}^t$. Further, we define the node as being in a congested state when the available sending bandwidth of node i at period t is less than the threshold of available sending bandwidth.

When node i is in a congested state at period t due to the long queue in the buffer of the node or the small available bandwidth for sending, the combination of Equations (7), (10) and (11) reveals that there is a serious deterioration in the network delay, packet loss rate, and throughput performance parameters at period t. For example, if PCO nodes No. 2 and No. 3 in Figure 1 are in congestion, more than half of the STA nodes from No. 3 to No. 9 need the above PCO nodes as relays, for uploading information to the CCO nodes, which will have deteriorated latency, throughput, and packet loss rate.

4. Network Establishment

The proposed algorithm consists of four phases: (1) the HPLC networking establishment phase; (2) the stabilization phase; (3) the HRF re-networking phase; (4) the HRF stabilization phase.

In phase (1), the CCO node broadcasts a networking request establishment frame to the STA node, and the STA node receives and replies to the STA node with a networking request confirmation frame, including the location of each STA node, the transmission bandwidth, and the size of the buffer.

The CCO node determines the location of the PCO nodes and the links between PCO nodes and STA nodes by using the mean shift algorithm based on the location information that is known for each STA node. The CCO node then detects the more remote nodes and connects them to the nearest PCO node. Moreover, to avoid affecting the quality of the STA nodes within the cluster due to the deterioration of the communication capability of the PCO nodes, it is considered to establish alternate paths between PCO nodes and STA nodes, which can divert the traffic as much as possible in case of congestion. Finally, we create ring links between the PCO nodes and connect the CCO nodes to each PCO node.

After establishing the HPLC networking, each STA node sends the power consumption information to the CCO node through the path determined by Dijkstra's algorithm.

In phase (2), PCO nodes report their respective cache occupied rate and available transmit bandwidth occupied rate to CCO nodes at regular intervals.

In phase (3), when the CCO node senses that a large number of PCO nodes' buffers are over-occupied or the available bandwidth for transmitting is too small, it broadcasts a re-networking frame to all the nodes. The PCO node sends the available transmit bandwidth and buffer occupancy of each node in the cluster to the CCO node in the form of a networking competition acknowledgment frame. If the waiting time is not exceeded, the CCO node will continue to wait for the campaign acknowledgment frame sent by the PCO node. If the wait time is exceeded, the CCO node identifies a new PCO node within each cluster based on the performance value calculated from the available transmit bandwidth and buffer occupancy. Since HPLC cannot change the established networking structure to optimize the network performance, we reorganize the network by using HRF communication to establish a new networking structure. The HRF network structure is similar to the HPLC network structure. It also requires detecting isolated nodes and connecting them to the nearest PCO node, establishing alternate paths, establishing ring links between PCO nodes, and connecting CCO nodes to each PCO node.

In phase (4), after the HRF networking establishment is completed, the STA node transmits the power consumption information to the CCO node using the path determined by the shortest hop path algorithm. The detailed procedures are shown in Figures 3 and 4.

Some key technologies in the above phases are explained as follows:

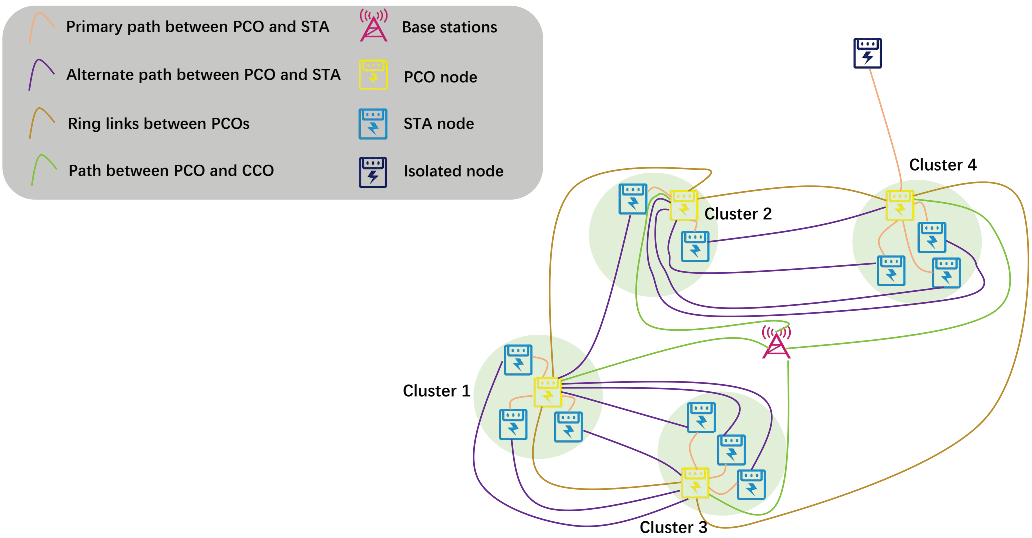

Figure 3. Networking process of the proposed scheme.

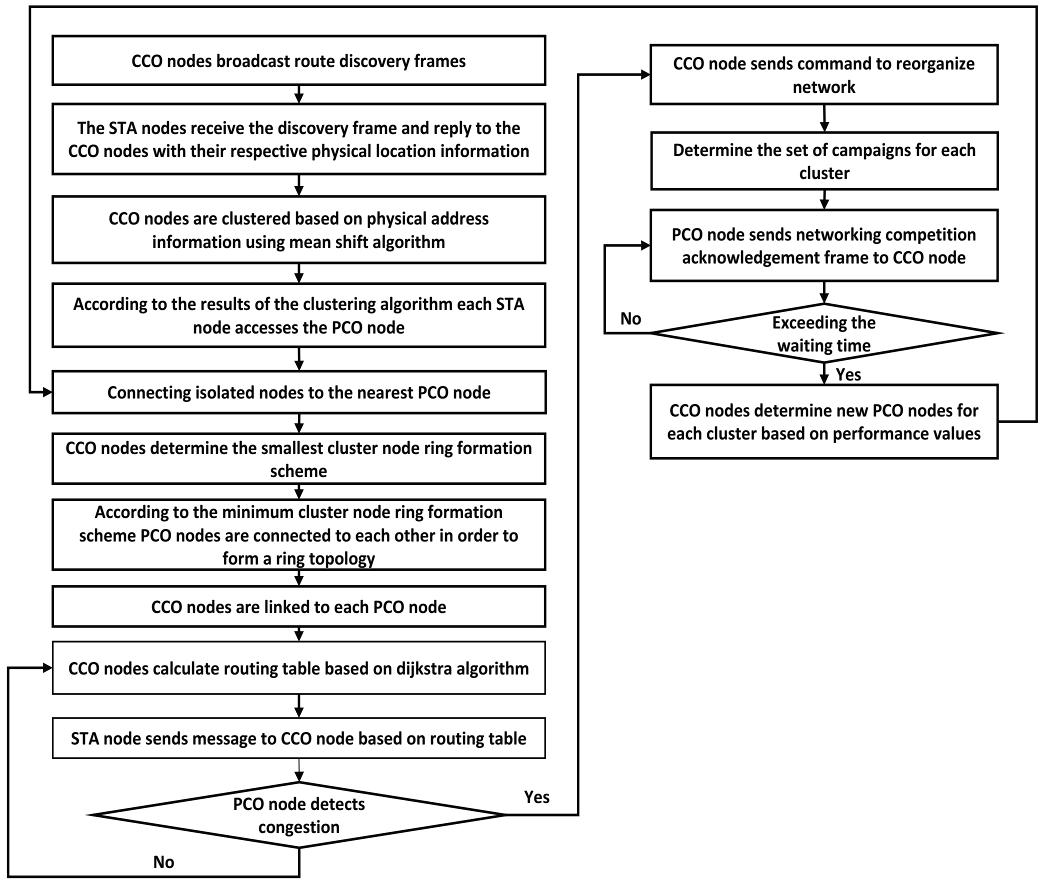

Figure 4. Dual-mode communication network flowchart.

4.1. Improved Mean Shift Algorithm

The basic idea of the mean shift algorithm is to continuously adjust the position of the STA nodes by shifting the mean value of the sample points in the feature space so that they shift toward the region of maximum local density. Specifically, the algorithm starts from the initial position, calculates the weights of the sample points under a given kernel function, and then allows the sample points to shift toward the weighted mean. This process is repeated until the sample points have drifted less than a certain threshold or a predetermined number of iterations have been reached.

Let the coordinates of the randomly selected initial center point, denoted as *center*, be given as (x_o, y_o). The radius of convergence is represented by *radius*.

To transform low-dimensional and nonfactual data points into high-dimensional fractions, the introduction of kernel functions enables computations to be accomplished directly in low-dimensional space. After transforming, the coordinates of all STA nodes are transformed from low-dimensional non-differentiable data to high-dimensional differentiable data, which can be clustered and classified. The initial center point is moved in the direction of increasing node density. The direction and distance of the movement are represented by the drift vector w, and the definition of w is given as follows:

$$w_i = \frac{e^{\|X_i - center\|^2}}{radius \cdot radius}, \tag{16}$$

where X_i are the coordinates of the STA nodes contained within a circle centered at *center* and with *radius* as the radius.

Using the kernel function allows STA nodes that are closer to the center point to have greater weight during the process of shifting, and the special points are prevented from affecting the shift on the center point.

Further, a new iterative formula for the position of the center of the circle is given as follows:

$$center^{(l+1)} = \frac{center^{(l)} + w_i \cdot X_i}{\sum_{i=1}^{n} w_i} \tag{17}$$

Traversing all STA nodes in the circle where the center point *center* is the center and *radius* is the radius, the shift vector is computed according to Equation (13). Then, the center point coordinates are updated according to Equation (14).

This center point shift process will end when the distance between $center^{(l+1)}$ and $center^{(l)}$ is less than the threshold value. The distance between the center point and the other identified cluster head needs to be calculated after the drifting process is finished. If the distance is less than a threshold value, the two center points need to be merged. Assuming that the coordinates of the two center points are (x_1, y_1) and (x_2, y_2), the coordinates of the merged center points are determined as follows:

$$center^{(merge)} = \left(\frac{x_1 + x_2}{2}, \frac{y_1 + y_2}{2} \right). \tag{18}$$

If there are still unvisited STA nodes within the dual-mode communication network at this time, the initial center point is randomly selected among these STA nodes by repeating the previously described steps until all STA nodes have been visited.

The detailed process is described in Algorithm A1 of Appendix A.1. The inputs of Algorithm A1 are the radius of convergence *radius* and the coordinates of the STA nodes *data_son_node*. The initial number of PCO nodes under each cluster *clustern*, their coordinate positions *clustercenter* and the PCO nodes to which the individual STA nodes are connected *Idx* are output by running Algorithm A1.

Since some STA nodes are spatially distributed remotely in the process of running Algorithm A1, which has no other STA nodes within the radius of convergence, these STA nodes will become their own PCO nodes and are defined as isolated nodes. On the one hand, isolated nodes do not play the role of relay nodes but are allocated communication resources as the PCO and STA nodes requirement. On the other hand, the single hop distance between the isolated node and the CCO node is too long, which causes exponential energy consumption. Based on the coordinate information, CCO nodes calculate the distance between these detected isolated PCO nodes and other non-isolated PCO nodes. To improve the communication resource utilization efficiency and reduce the energy consumption of the dual-mode communication network as much as possible, the PCO node closest to the isolated node is selected from the set of PCO nodes, which is calculated by Algorithm A1, and it will be connected to the isolated node. The detailed procedure is described in Algorithm 1.

After connecting the isolated PCO node to the nearest non-isolated PCO node, the CCO node updates the number of PCO nodes *clustern*, PCO node coordinates *clustercenter*, and the PCO node accessed by each STA node *Idx* information for the whole dual-mode communication network.

4.2. Alternate Path Establishment

STA nodes connected to only one PCO node will be vulnerable to the effects of congestion. Therefore, we consider establishing alternate paths in the event of congestion that move traffic to areas that are not affected by congestion.

The CCO node connects each STA node to the nearest PCO node except the already connected PCO node based on the STA node and PCO node coordinate information. The detailed procedure is described in Algorithm 2. Algorithm 2 is executed by inputting the number of PCO nodes, PCO node coordinates, number of STA nodes, STA node coordinates, and PCO nodes accessed by each STA node, which selects alternate PCO nodes that are closer to being accessed.

After establishing the path between the PCO and STA nodes, we establish the ring path between the PCO nodes. Finally, all the PCO nodes are connected to the CCO nodes.

Algorithm 1 Isolated PCO node access algorithm

Input: *clustern*,*clustercenter*,*Idx*,*nodes_number*,*data_son_node*
for $i \leftarrow 1 : nodes\_number$ **do**
  for $j \leftarrow 1 : clustern$ **do**
    if $(data\_son\_node(i,1) == clustercenter(j,1))$ $\&\&(data\_son\_node(i,2) == clustercenter(j,2))$ **then**
      $state\_cluster(j,:) \leftarrow [1,i]$
      for $K \leftarrow 1 : clustern$ **do**
        if $Idx(k) > j$ **then**
          $Idx(k) \leftarrow Idx(k) - 1$
        end if
      end for
    end if
  end for
end for
$temp\_clustern \leftarrow clustern$
for $i \leftarrow 1 : temp\_clutern$ **do**
  if $state\_cluser(i,1) == 1$ **then**
    $clustercenter(i,:) \leftarrow []$
    $clustern \leftarrow clustern - 1$
    $temp\_distance \leftarrow \text{inf}$
    for $j \leftarrow 1 : clustern$ **do**
      $cluser\_node\_distance \leftarrow$ *distance between isolated PCO node and other PCO node*
      if $(cluster\_node\_distance < temp\_distance)\&\&(\text{cluster\_node\_distance} \neq 0)$ **then**
        $temp\_distance \leftarrow cluster\_node\_distance$
        $Idx(state\_cluster(i,2)) \leftarrow j$
        $Idx(state\_cluster(i,2)) \leftarrow j$
      end if
    end for
  end if
end for
Output: *clustern*,*clustercenter*,*Idx*

Algorithm 2 Access to alternate PCO node Algorithm

Input: *clustern*,*clustercenter*,*Idx*,*nodes_number*,*data_son_node*
for $i \leftarrow 1 : nodes\_number$ **do**
  $cluster\_node\_\min\_distance \leftarrow \text{inf}$
  for $j \leftarrow 1 : clustern$ **do**
    $cluser\_node\_sum\_distance \leftarrow$ *distance between STA node and PCO node*
    if $(Idx(i) \neq j)\&\&(cluster\_node\_sum\_distance < cluster\_node\_\min\_distance)$ **then**
      $cluster\_node\_\min\_distance \leftarrow cluster\_node\_sum\_distance$
      $Idx\_spare(i) \leftarrow j$
    end if
  end for
end for
Output: *Idx_spare*

5. Load Balancing and Routing

5.1. PCO Node Election

If the PCO node detects that its buffer is excessively occupied or the available bandwidth for sending is insufficient, it promptly reports this issue to the CCO. After receiving the information, the CCO node issues a re-network command to all the nodes. All PCO nodes and STA nodes reply to the central node CCO with a re-networking confirmation frame after receiving the re-networking command, and the central node CCO starts to re-network using the HRF communication method after receiving the re-networking confirmation frames from all PCO nodes and STA nodes. If we do not receive the re-networking confirmation frames from some of the STA nodes and PCO nodes, we assume that these nodes are not able to access the network for a short period. The CCO node removes the above mentioned nodes from the networking topology during the re-networking process.

To simplify the complexity of the problem studied in this paper, we assume that the CCO node receives the re-grouping confirmation frames sent by all STA nodes and PCO nodes. We adopt a competitive approach to identify the new PCO nodes for re-networking.

During the contention time, the CCO node sends the networking competition frame to the PCO nodes, and each PCO node sends its respective buffer occupancy and transmit bandwidth occupancy to the CCO node as networking competition acknowledgment frame. After exceeding the competition time, the CCO node calculates the $performance$ values of the nodes in the campaign set to identify the STA nodes that become PCO nodes as follows:

$$performance = \frac{\min(output\_all)}{output\_all(idx\_candidate(j,i))} \cdot \frac{buffer\_occupancy\_all(idx\_candidate(j,i))}{\max(buffer\_occupancy\_all)}, \tag{19}$$

where $output\_all$ is the transmit available bandwidth and $buffer\_occupancy\_all$ is the buffer occupancy size. By adding a normalization factor, it is possible to evaluate the effect of different magnitudes for transmitting available bandwidth and buffer occupancy in one equation for $performance$. The smaller value of $performance$ obtained from the calculation indicates that the system will obtain better performance by selecting this STA node as the PCO node, while the opposite indicates that the system will not be able to get better performance. The detailed procedure is described in Algorithm 3. The PCO nodes obtained by running Algorithm 3 will be re-networked.

5.2. Establishment of Shortest Hop Routing

After the HRF network is established, each STA node uses the Dijkstra algorithm to select the path with the shortest number of hops for sending their respective power consumption information to the CCO node. The rationale behind utilizing the path with the shortest number of hops lies in the fact that network performance metrics, such as delay, packet loss rate, throughput, etc., exhibit a strong correlation with the number of nodes traversed. The larger the number of nodes involved, the more these metrics tend to deteriorate. Therefore, opting for the shortest path helps to mitigate the adverse effects on these performance parameters, resulting in a more efficient data delivery process. The detailed procedure is described in Algorithm A2 of Appendix A.1.

Algorithm 3 PCO node campaign algorithm

Input: $clustern, idx\_candidate, data\_all, output\_all, buffer\_occupancy\_all$

for $i \leftarrow 1 : clustern$ **do**
  $best\_performance \leftarrow inf$
  for $j \leftarrow 1 : length(idx\_candidate(find(idx\_candidate(:,i) \neq 0)))$ **do**
    for $k \leftarrow 1 : length(idx\_candidate(find(idx\_candidate(:,i) \neq 0)))$ **do**

$$hrf\_candidate\_dis\tan ce(j,k) = \left(\left(\begin{array}{l} data\_all(idx\_candidate(j,i),1) \\ -data\_all(idx\_candidate(k,i),1) \end{array} \right)^2 + \left(\begin{array}{l} data\_all(idx\_candidate(j,i),2) \\ -data\_all(idx\_candidate(k,i),2) \end{array} \right)^2 \right)^{\frac{1}{2}}$$

    end for
  end for
  for $j \leftarrow 1 : length(idx\_candidate(find(idx\_candidate(:,i) \neq 0)))$ **do**
    $hrf\_candidate\_all\_performance \leftarrow 0$
    for $k \leftarrow 1 : length(idx\_candidate(find(idx\_candidate(:,i) \neq 0)))$ **do**

$$hrf\_candidate\_all\_performance \leftarrow hrf\_candidate\_all\_performance + \left(\frac{\min(output\_all)}{output\_all(idx\_candidate(j,i),1)} \cdot \frac{buffer\_occupancy\_all(idx\_candidate(j,i),1)}{\max(buffer\_occupancy\_all)} \right)$$

    end for
    if $hrf\_candidate\_all\_performance < best\_performance$ **then**
      $best\_performance \leftarrow hrf\_candidate\_all\_performance$
      $hrf\_clustern \leftarrow data\_all(idx\_candidate(j,1))$
      $hrf\_cluster\_id(i) \leftarrow idx\_candidate(j,i)$
    end if
  end for
end for

Output: $hrf\_clustercenter, hrf\_cluster\_id$

6. Experimental Results and Analysis

6.1. Simulation Settings

In this section, we verify the performance of the proposed algorithms by some simulations on MATLAB 2022b. We refer to previous work on power Internet of Things routing [44–46] and list the main simulation parameters in Table 1. The scale of the network in Section 6.5 is extended from 60 m × 60 m as in Table 1 to 240 m × 240 m. Larger and larger network sizes require more and more network nodes for coverage, so correspondingly, we extend the number of STA nodes from 30 to 120, as shown in Table 1. Similarly, the radius of convergence of the mean shift algorithm is gradually increased from 16.2 m to 64.8 m in our simulations. The bandwidth of the STA node and the number of bits contained in a packet are set to 8 Mbps and 128 Kbps, respectively. In order to represent the difference in the available transmit bandwidth of different nodes in the simulation, we set the available transmit bandwidth of the high transmit rate node and normal node to 0.9375 and 0.80, respectively. Similarly, we set the buffer occupancy to 0.10 and 0.30 for low-occupancy nodes and normal nodes, respectively. Figures 5 and 6 show the structural diagrams of the simulated network before and after re-grouping by adopting the proposed scheme, respectively. In the simulation process, we randomly generate fifty STA nodes denoted by blue solid circles and CCO nodes denoted by black solid circles with coordinates (70,50) in a spatial area of 100 × 100 m as shown in Figures 5 and 6. The yellow solid line indicates the link from the CCO node to the PCO node. The red solid line indicates the path between the PCO and STA nodes obtained by running Algorithm A1 and Algorithm 1. The blue solid line indicates the alternate path between the PCO and STA nodes that have obtained by running Algorithm 2. The purple solid line indicates the ring link between the PCO nodes by running Algorithm 3.

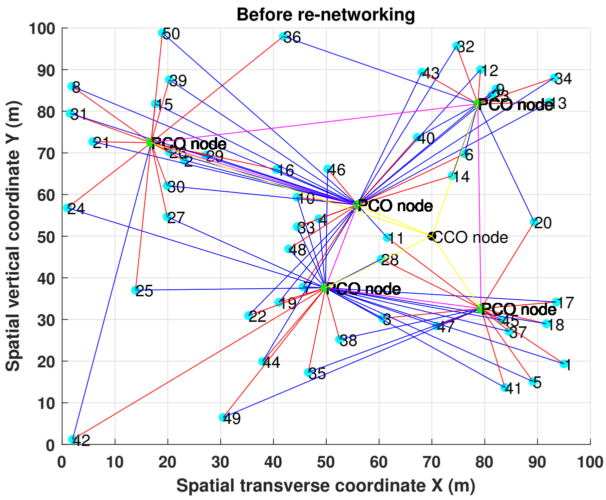

Figure 5. The network simulation diagram before networking again.

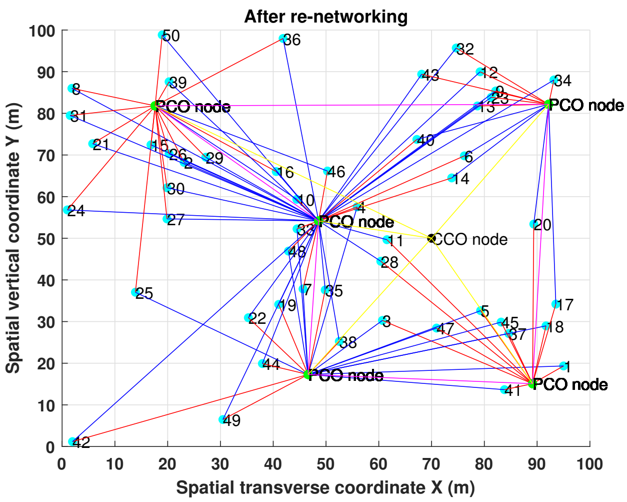

Figure 6. The network simulation diagram after networking again.

To evaluate the performance, the proposed algorithm is compared with the classical Dijkstra's algorithm, SEAR algorithm, classical LEACH algorithm, and DCBSRP algorithm for the metrics that can evaluate the routing performance of the dual-mode communication network, including latency, throughput, and packet loss rate.

In the simulation, the Dijkstra algorithm will determine the path with the shortest number of hops before re-networking. The SEAR algorithm will improve the congested node's available transmission bandwidth. The LEACH algorithm will determine the new PCO node before re-networking based on the probability generated by the ratio of PCO nodes to all nodes and the number of times they have become passed PCO nodes. The DCBSRP algorithm confirms the PCO nodes by the number of RREPs when re-networking.

The proposed scheme adds the PCO node election mechanism compared to the classical Dijkstra algorithm and SEAR algorithm. When Dijkstra's algorithm is applied, information can be only sent from STA nodes to CCO nodes by using the existing very poor performance networking method. The SEAR algorithm can recover the transmit available bandwidth of a node affected by congestion. The proposed scheme optimizes the PCO election compared to the DCBSRP algorithm and LEACH algorithm. The LEACH algorithm randomly selects the STA node as the PCO node for the re-networking phase, which has a high probability that it will be selected to a PCO node with large buffer occupancy and small available bandwidth for sending. The DCBSRP algorithm does not focus on the transmitting capability of a PCO node, although it can select a PCO node with a smaller buffer occupancy. The scheme does not consider the impact of buffer occupancy and the available bandwidth for nodes to send on the system performance in an integrated manner. Because we can select the PCO nodes with smaller cache occupancy and larger sending available bandwidth, our proposed scheme has better performance compared to the previous schemes.

By varying the simulation parameters of the network, it is possible to evaluate the superiority of the proposed scheme over previous schemes under different scenarios of heterogeneous networks with dual-mode communication. We need to simulate and verify that in the presence of congestion at the PCO nodes, which means that there is a deterioration in the available bandwidth for sending and buffer occupancy compared to the normal case, the proposed scheme has a significant improvement in delay, throughput, and packet loss compared to the previous work.

To evaluate the overall performance of the network, the average values of delay, packet loss rate, and throughput from each STA node to the CCO node are calculated.

Table 1. Simulation parameters.

Parameter	Value
Area	60 m × 60 m, 80 m × 80 m, 100 m × 100 m, 120 m × 120 m, 140 m × 140 m, 160 m × 160 m, 180 m × 180 m, 200 m × 200 m, 220 m × 220 m
BS coordinates	(56 m, 57 m)
Number of STA nodes	30, 40, 50, 60, 70, 80, 90, 100, 110, 120
radius	16.2 m, 21.6 m, 27 m, 32.4 m, 40.6 m, 42.0 m, 50.4 m, 54 m, 71.5 m
STA node bandwidth	8 Mbps
Number of bits contained in a packet	128 Kbps
Available transmit bandwidth factor of normal node	0.80
Available transmit bandwidth factor of high transmit rate node	0.9375
Buffer occupancy of normal node	0.30
Buffer occupancy of low occupancy nodes	0.10

6.2. Case for Different Number of PCO Nodes in Congested State

This section shows and analyzes the performance of three networking approaches, which are alternative paths only, alternative paths combined with campaigning mechanism, and traditional tree-type structure, when the number of PCO nodes in congested state is different. Figure 7 shows the average delay for different number of PCO nodes affected by congestion when the number of packets sent by the STA node is 150, the congested node buffer occupancy is 0.8, buffer capacity is 45, and the congested node available bandwidth factor is 0.32 at different number of packets sent by the STA node. As more and more PCO nodes are in congested state, the average delay of the network is increasing. The traditional tree structure has the largest delay and the fastest deterioration of the delay. This is because the traditional tree structure is the least robust and the STA nodes are connected to only one PCO node. The PCO node in a congested state will directly affect all the STA nodes accessing it. The delay performance of the alternate-path-only approach is better than the traditional tree structure. This is because setting up alternate paths enables an STA node to communicate with a CCO node through two different PCO nodes. If one of the PCO nodes is in the congested state, it is able to maintain the communication to the CCO node through the other PCO node with better performance. However, when the number of PCO nodes in a congested state reaches five, the performance of the alternate-path-only approach will deteriorate to the same extent as the traditional tree structure approach. This is because when the number of PCO nodes in congested state is high, it is very likely that both PCO nodes accessed by the STA node will be in congested state. The alternate-path-only approach will not be able to establish a better performing link to the CCO node. The best performance was obtained by combining the alternate path with the PCO election mechanism. This is because no matter what the number of PCO nodes in congested state is, it can always get the PCO nodes that are not in congested state to re-network through election. Further, the STA nodes are able to communicate with the CCO nodes through the uncongested PCO nodes.

Figure 8 shows the throughput for different number of PCO nodes in congested state when the number of packets sent by the STA node is 150, the congested node buffer occupancy is 0.8, buffer capacity is 45, and the congested node available bandwidth factor is 0.32 at different number of packets sent by the STA node. As the number of PCO nodes in a congested state increases, the throughput of the network becomes smaller. The traditional tree structure approach has the worst throughput and the fastest deterioration. Only the alternate path approach can optimize the throughput performance to some extent as more and more PCO nodes are in a congested state. But when the number of PCO nodes in a congested state exceeds a certain number, the throughput performance will be less different from the traditional tree structure approach. The approach combining alternate paths and campaigning mechanism achieves large throughput at different number of PCO nodes in a congested state.

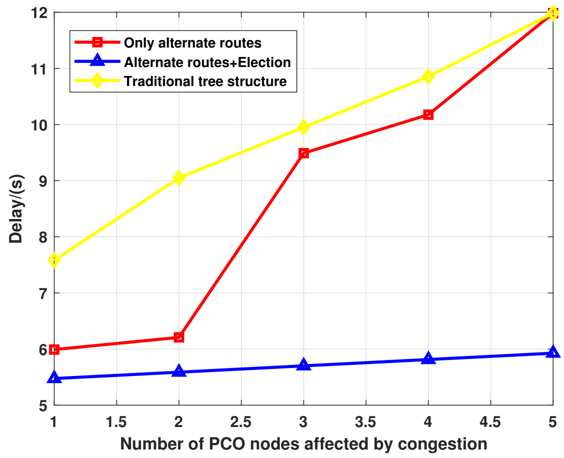

Figure 7. The average delay for different numbers of PCO nodes in congested state.

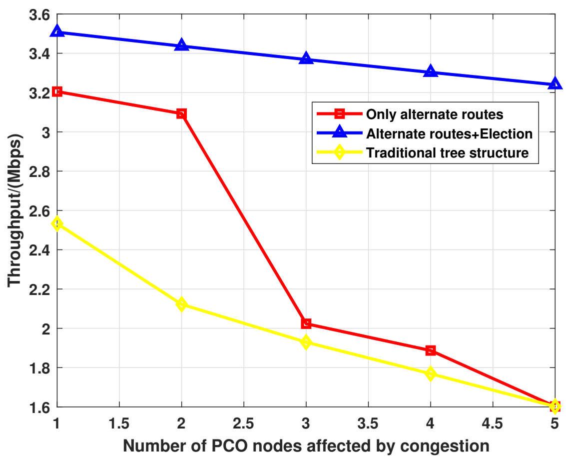

Figure 8. The average throughput for different numbers of PCO nodes in congested state.

Figure 9 shows the packet loss rate for different numbers of PCO nodes in a congested state when the number of packets sent by the STA node is 150, the congested node buffer occupancy is 0.8, buffer capacity is 45, and the congested node available bandwidth factor is 0.32 at different number of packets sent by the STA node. As the number of PCO nodes in a congested state increases, the packet loss rate of the network becomes larger. The traditional tree structure approach has the worst packet loss rate and the fastest deterioration. Only the alternate path approach can optimize the packet loss rate performance to some extent as more and more PCO nodes are in congested state. But when the number of PCO nodes in congested state exceeds a certain number, the packet loss rate performance will be less different from the traditional tree structure approach. The approach combining alternate paths and campaigning mechanism achieves small packet loss rate at different numbers of PCO nodes in a congested state.

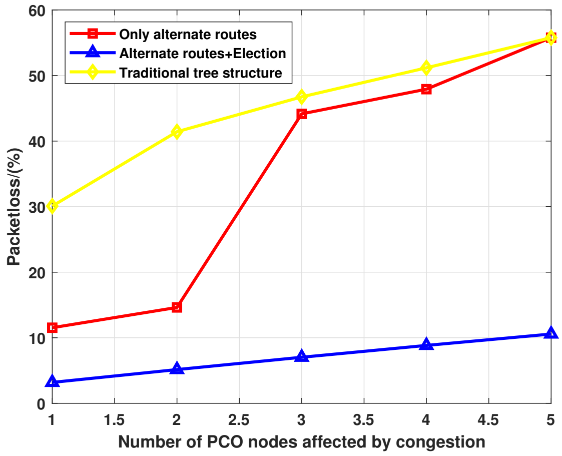

Figure 9. The average packet loss rate for different numbers of PCO nodes in congested state.

6.3. Case for Different Numbers of Packets to Be Sent by STA Nodes

This section shows and analyzes the performance of the network in terms of delay, throughput, and packet loss rate of different methods when STA nodes send different number of packets. Figure 10 shows the average delay when the congested node buffer occupancy is 0.8, the network scale is 100 m × 100 m, the number of STA nodes is 50, the buffer capacity is 45, and the congested node available bandwidth factor is 0.32 at the different number of packets sent by the STA node. This is because the transmission process takes more time for each node to transmit these packets to the next node, as the number of packets to be sent by the STA increases. Since the traditional Dijkstra's algorithm can only transmit the excess packets generated by congestion to the CCO nodes by increasing the processing time, it is affected by congestion, resulting in a significantly larger delay than other schemes. The reason why the SEAR scheme is significantly better than the Dijkstra algorithm but worse than the other schemes is that it can only recover the available bandwidth for sending from the nodes to the nodes in a limited way and it does not solve the problem of excessive buffer occupancy. To ensure optimal buffer occupancy, the DCBSRP algorithm will elect some STA nodes with poor sending rates as PCO nodes, resulting in a delay that is only better than the Dijkstra and SEAR algorithms. The DCBSRP method makes only the nodes with lower buffer occupancy PCO nodes without considering the size of the available sending rate of the node. Some PCO nodes with very poor available sending rates can seriously worsen the communication delay. Therefore, the LEACH algorithm with randomly selected PCO nodes will perform better than the DCBSRP algorithm in terms of latency. The proposed scheme PCO node has a relatively strong ability to process and send data, which can be processed faster in the case of the same number of packets.

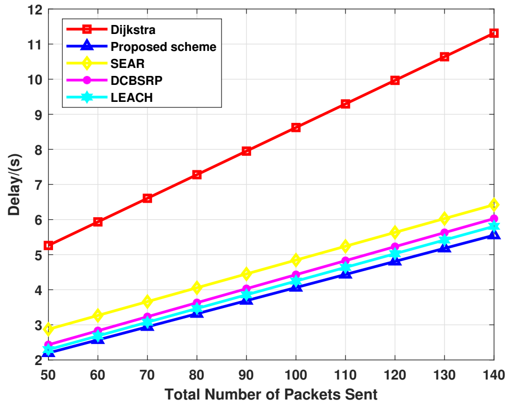

Figure 10. The Average delay for different number of packets sent.

Figure 11 shows the average throughput when the congested node buffer occupancy is 0.8, the network scale is 100 m × 100 m, the number of STA nodes is 50, the buffer capacity is 45, and the congested node available bandwidth factor is 0.32 at the different numbers of packets sent by the STA node. As the number of packets required to be sent increases, the number of packets received increases and the throughput increases significantly.

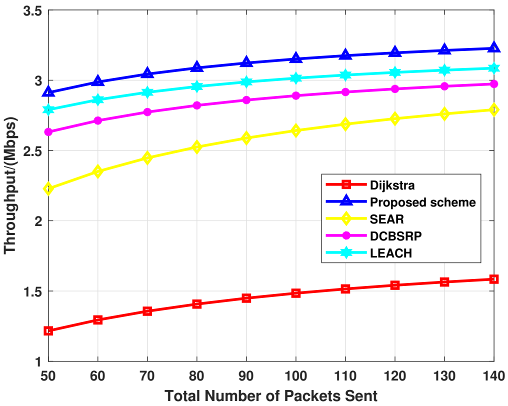

Figure 11. The average throughput for different numbers of packets sent.

Figure 12 shows the average packet loss rate when the congested node buffer occupancy is 0.8, the network scale is 100 m × 100 m, the number of STA nodes is 50, buffer capacity is 45, and the congested node available bandwidth factor is 0.32 at different number of packets sent by the STA node. The increase in the number of packets that need to send leads to more queue length over the buffer at each node, so the number of packets received by the CCO decreases and the average packet loss rate of the network increases.

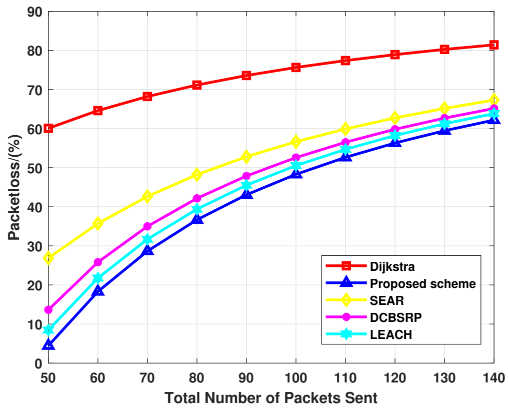

Figure 12. The average packet loss for different numbers of packets sent.

6.4. Case for Different Congested Node Available Bandwidths

This section shows and analyzes the performance of the network in terms of delay, throughput, and packet loss rate of different methods at different congested node available bandwidths. Figure 13 shows the average delay when the congested node buffer occupancy is 0.8, the network scale is 100 m × 100 m, the number of STA nodes is 50, buffer capacity is 45, and the number of packets sent by the STA node is 55 at different congested node available bandwidths. The more bandwidth available for the congested node causes the node to be more capable of sending information, and hence the information is transmitted faster, making the average delay of the network routing smaller. The LEACH algorithm, the DCBSRP algorithm, and the proposed scheme have significant advantages over Dijkstra's algorithm and the SEAR algorithm. As the bandwidth available to the congested nodes increases, the delay, packet loss rate, and throughput of the former do not deteriorate as much as the latter because the former uses the PCO competition mechanism, which tries to avoid the congested nodes from affecting the entire network. As the available bandwidth factor of congested nodes decreases from 0.76 to 0.44, the average increased latency of the Dijkstra and SEAR algorithms is about 1.53 s, while the average increases in the DCBSRP algorithm, the LEACH algorithm, and the proposed scheme are about 0.15 s. It can be recognized that the use of the HRF re-networking approach over the traditional single-mode communication can be used to obtain a smaller network routing delay in the event of available bandwidth decrease at the nodes due to congestion.

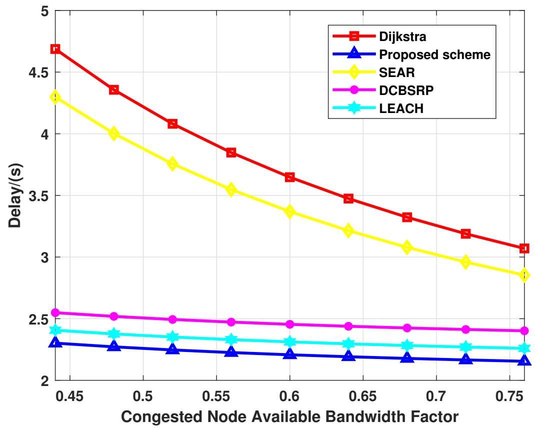

Figure 13. The average delay for different congested node available bandwidth factors.

Figure 14 shows the average throughput when the congested node buffer occupancy is 0.8, the network scale is 100 m × 100 m, the number of STA nodes is 50, buffer capacity is 45, and the number of packets sent by the STA node is 55 at different congested node available bandwidths. As the available bandwidth factor of the congested node decreases from 0.76 to 0.44, the throughput of the Dijkstra algorithm and SEAR algorithm decreases by approximately 0.81 Mbps on average, and the DCBSRP algorithm, LEACH algorithm, and the proposed scheme decrease by approximately 0.24 Mbps on average. This is because the ability of the entire network to route the information is improved and the CCO receives more power consumption information per unit of time sent from the STA, as the available bandwidth of the congested nodes increases. Based on the above analysis, the throughput of the network also increases with the increase in the available bandwidth for the congested nodes.

Figure 15 shows the average packet loss rate when the congested node buffer occupancy is 0.8, the network scale is 100 m × 100 m, the number of STA nodes is 50, buffer capacity is 45, and the number of packets sent by the STA node is 55 at different congested node available bandwidths. As the available bandwidth factor for sending from congested nodes decreases from 0.76 to 0.44, the packet loss rates of Dijkstra's algorithm and SEAR algorithm improve by about 24.17% on average, and the DCBSRP algorithm, LEACH algorithm, and the proposed scheme improve by about 5.65% on average. As the available bandwidth of the congested node increases, the congestion in the buffer of the node is reduced, and the ability of the entire network to process the information is increased.

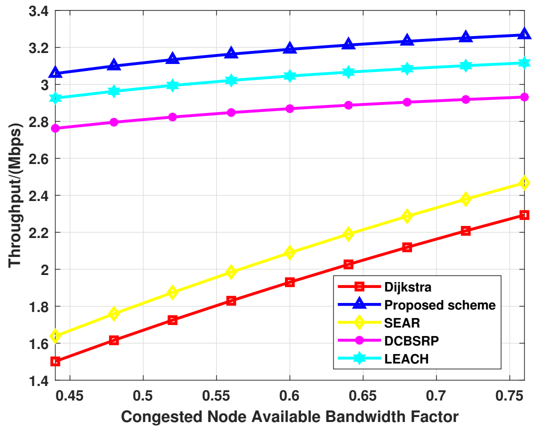

Figure 14. The Average throughput for different congested node Available Bandwidth Factors.

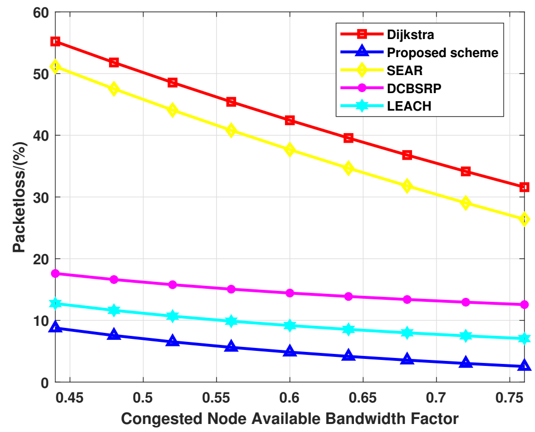

Figure 15. The average packet loss for different congested node available bandwidth factors.

6.5. Case for Different Congestion Buffer Occupancies

This section shows and analyzes the performance of the network in terms of delay, throughput, packet loss rate of different methods at different congested node buffer occupancies. Figure 16 shows the average delay when the congested node available bandwidth factor is 0.4, the network scale is 100 m × 100 m, the number of STA nodes is 50, buffer capacity is 45, and the number of packets sent by the STA node is 50 at different congested node buffer occupancies. As the buffer occupancy of the congested node increases from 0.4 to 0.85, the delay of the Dijkstra algorithm increases by approximately 1.01s, the SEAR algorithm experimentally increases by approximately 0.45 s, and the DCBSRP algorithm, the LEACH algorithm, and the proposed scheme increase on average approximately 0.09 s. This is because increased buffer occupancy increases queue length, which in turn increases queuing delay.

Figure 17 shows the average throughput when the congested node available bandwidth factor is 0.4, the network scale is 100 m × 100 m, the number of STA nodes is 50, buffer capacity is 45, and the number of packets sent by the STA node is 50 at different congested node buffer occupancies. As the buffer occupancy of the congested node increases from 0.4 to 0.85, the throughput of the Dijkstra algorithm and SEAR algorithm decreases by approximately 0.33 Mbps on average, and the DCBSRP algorithm, the LEACH algorithm, and the proposed scheme decrease on average approximately 0.11 Mbps. This is because the increase in buffer occupancy results in fewer resources in the network that can be allocated to the transmission of power consumption information, and the CCO receives less information per unit of time, which means that the throughput decreases.

Figure 18 shows the average packet loss rate when the congested node available bandwidth factor is 0.4, the network scale is 100 m × 100 m, the number of STA nodes is 50, buffer capacity is 45, and the number of packets sent by the STA node is 50 at different congested node buffer occupancy. As the buffer occupancy of the congested node increases from 0.4 to 0.85, the packet loss rates of the Dijkstra algorithm and SEAR algorithm decrease by approximately 11.07%, and the DCBSRP algorithm, the LEACH algorithm, and the proposed scheme decrease on average by approximately 3.77%. This is because the increase in buffer occupancy leads to more buffer queue length exceeding the buffer size, and more packets are dropped, which means that the packet loss rate is greater.

The best performance is obtained for the proposed schemes in Figures 16–18. The reason is that the schemes try to elect PCO nodes with small buffer occupancy and large transmit available bandwidth, which prevents the nodes in the congested state from becoming PCO nodes. Even though the queue length of the congested node's buffer increases the risk of queuing delay and packet loss of congested nodes, the proposed scheme tries to limit the impact in a limited area as much as possible through not allowing the congested node to become a key player in transmitting information within the dual-mode communication network.

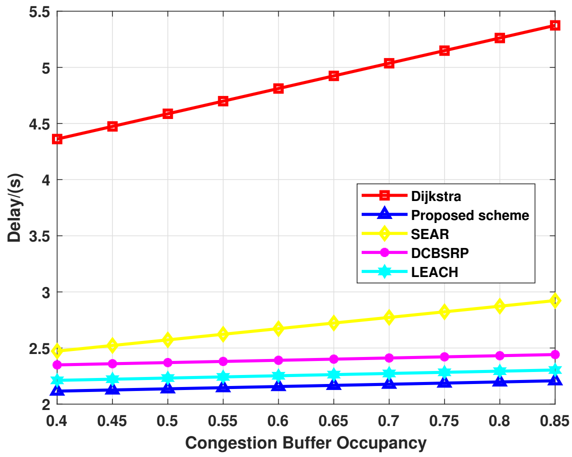

Figure 16. The average delay for different congestion buffer occupancies.

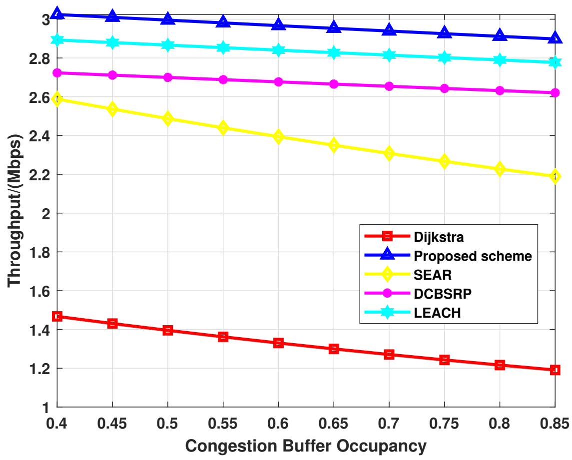

Figure 17. The average throughput for different congestion buffer occupancies.

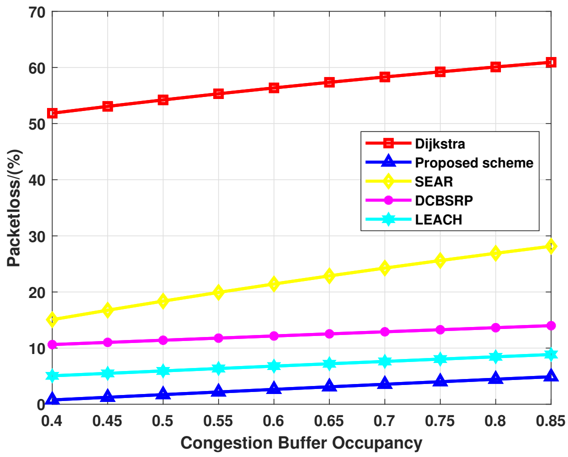

Figure 18. The average packet loss for different congestion buffer occupancies.

Dijkstra algorithm and SEAR algorithm are mainly suitable to be used by single-mode HPLC communication. Due to the limitation of the fixed HPLC network, even if it is affected by severe congestion, the congested node still has to play a key role in the network routing. Compared with the Dijkstra algorithm, which is similar to a hands-off approach, the SEAR algorithm recovers the transmission rate of the congested node as much as possible, but it cannot solve the challenges of excessive queuing delay and increased risk of packet loss caused by the increasing buffer occupancy of the congested node. The LEACH algorithm and DCPSRP algorithm, although using a similar PCO node election mechanism similar to the proposed scheme, are unable to elect a PCO node that takes into account both the buffer size and the available bandwidth for sending. Unlike the above algorithms, the proposed scheme is able to elect a PCO node that considers both the buffer size and the available sending bandwidth.

6.6. Case for Different Buffer Capacities

This section shows and analyzes the performance of the network in terms of delay, throughput, packet loss rate of different methods at different buffer capacities. Figure 19 shows the average delay when the congested node available bandwidth is 0.32, the network scale is 100 m × 100 m, the number of STA nodes is 50, congested node buffer occupancy is 0.8, and the number of packets sent by the STA node is 10 at different buffer capacities. When the capacity of each cache is changed from the one that can accommodate 10 packets to the one that can accommodate 55 packets, the delay of the Dijkstra algorithm increases approximately 1.90s, the delay of the SEAR algorithm increases approximately 0.90 s, and the delay of the DCBSRP algorithm, LEACH algorithm, and the proposed scheme increases on average by approximately 0.37 s. This is because the increase in the capacity of the buffer leads to an increase in the number of packets, which requires more time for the node to process.

Figure 20 shows the average throughput when the congested node available bandwidth is 0.32, the network scale is 100 m × 100 m, the number of STA nodes is 50, congested node buffer occupancy is 0.8, and the number of packets sent by the STA node is 10 at different buffer capacities. After the queue length increases in the buffer, the CCO receives fewer packets per unit of time. When the buffer capacity is increased from 10 packets to 55 packets, the throughput of the Dijkstra and SEAR algorithms decreases approximately 0.68 Mbps on average, and the throughput of the DCBSRP algorithm, LEACH algorithm, and the proposed scheme decreases approximately 0.45 Mbps on average.

Figure 21 shows the average packet loss rate when the congested node available bandwidth is 0.32, the network scale is 100 m × 100 m, the number of STA nodes is 50, congested node buffer occupancy is 0.8, and the number of packets sent by the STA node is 10 at different buffer capacities. When the buffer capacity is increased from being able to accommodate 10 packets to being able to accommodate 55 packets, the packet loss rates of the Dijkstra algorithm and SEAR algorithm approximately increase by 20.25% on average, and the DCBSRP algorithm, the packet loss rates of the LEACH algorithm, and the proposed scheme approximately increase 15.53% on average. This is because of a significant increase in the possibility of packet loss where the data stored in the buffer exceeds the size of the buffer within the nodes, which leads to an increase in the average packet loss rate across the network. In addition, the proposed scheme has optimal performance in delay, throughput, and packet loss rate.

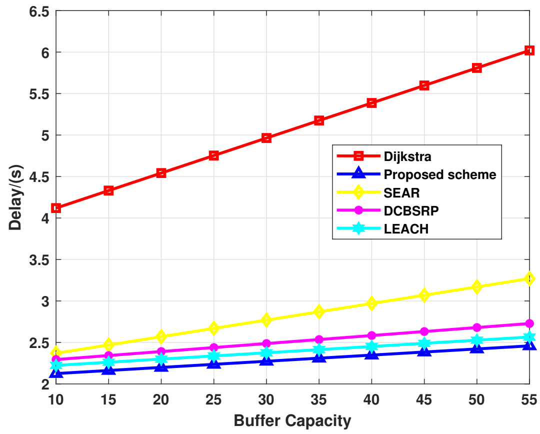

Figure 19. The average delay for different buffer capacities.

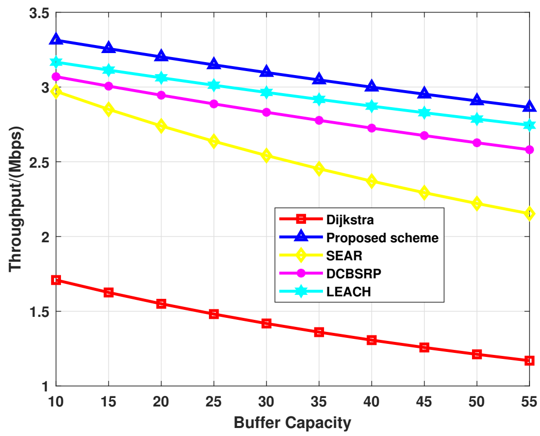

Figure 20. The average throughput for different buffer capacities.

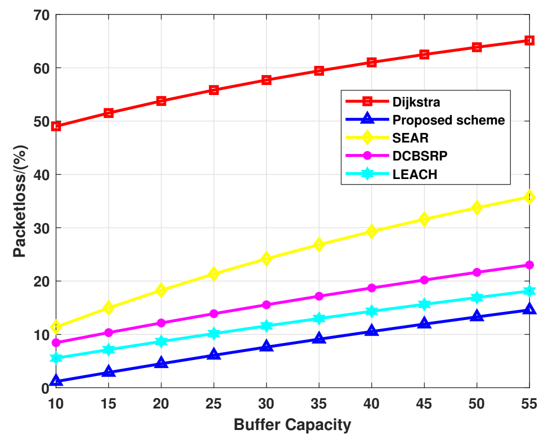

Figure 21. The average packet loss for different buffer capacities.

6.7. Case for Different Scales of Network

This section shows and analyzes the performance of the network in terms of delay, throughput, and packet loss rate of different methods at different scales of the network. Figure 22 shows the average delay when the congested node available bandwidth is 0.32, buffer capacity is 45, congested node buffer occupancy is 0.8, and the number of packets sent by the STA node is 55 at different scales of the network. When the scale of the network is increased from 60 m to 240 m, the delays of the LEACH algorithm, the DCBSRP algorithm, and the proposed algorithm decrease in general, while the delays of the Dijkstra algorithm and SEAR algorithm increase in general. The reason for the above phenomenon is that the LEACH algorithm, the DCBSRP algorithm, and the proposed algorithm are able to re-network the network so that PCO nodes in a congested state can be avoided to varying degrees, and the gain resulting from this avoidance is enhanced as more and more normally functioning STA nodes are added to the simulation. However, the SEAR algorithm and Dijkstra algorithm do not have the step of networking again, and the PCO nodes in a congested state will keep affecting a large number of STA nodes sending information to the CCO nodes on the link. As the network size continues to grow, there will be more and more STA nodes affected by the above, so the delay performance of the Dijkstra and SEAR algorithms will continue to deteriorate. Finally, the proposed scheme obtains the optimal delay performance compared to the comparison scheme. This is due to the fact that the proposed scheme not only incorporates an election mechanism but also a mechanism that balances the available transmit bandwidth and buffer occupancy.

Figure 23 shows the average throughput when the congested node available bandwidth is 0.32, buffer capacity is 45, congested node buffer occupancy is 0.8, and the number of packets sent by the STA node is 55 at different scales of the network. When the scale of the network is increased from 60 m to 240 m, the throughput of the LEACH algorithm, the DCBSRP algorithm, and the proposed algorithm increases in general, while the throughput of the Dijkstra algorithm and SEAR algorithm decreases in general. On the other hand, the proposed scheme obtains the optimal throughput performance compared to the comparison scheme.

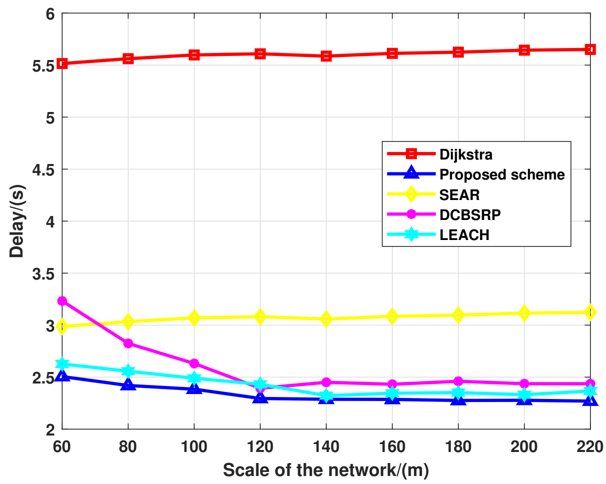

Figure 22. The average delay for different scales of the network.

Figure 24 shows the average packet loss rate when the congested node available bandwidth is 0.32, buffer capacity is 45, congested node buffer occupancy is 0.8, and the number of packets sent by the STA node is 55 at different scales of the network. When the scale of the network is increased from 60 m to 240 m, the packet loss rates of the LEACH algorithm, the DCBSRP algorithm, and the proposed algorithm decrease in general, while the packet loss rates of the Dijkstra algorithm and SEAR algorithm increase in general. On the other hand, the proposed scheme obtains the optimal packet loss rate performance compared to the comparison scheme.

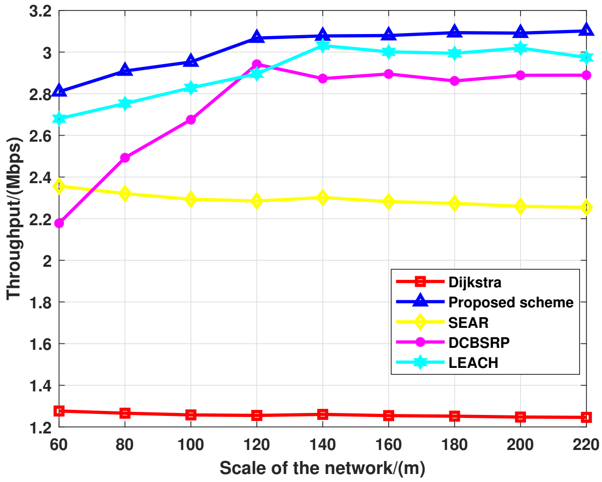

Figure 23. The average throughput for different scales of the network.

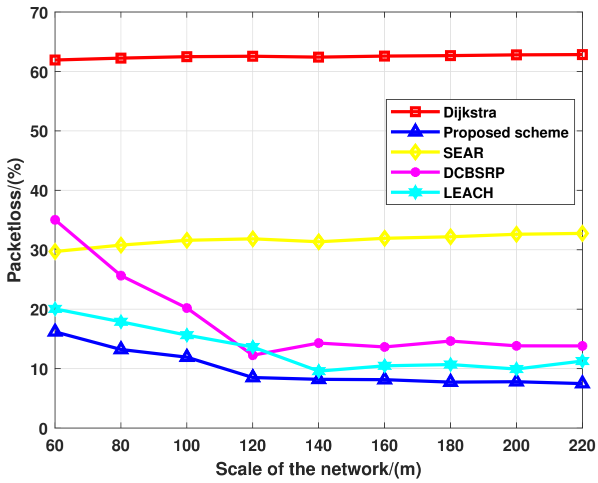

Figure 24. The average packet loss for different scales of the network.

7. Discussion

The proposed scheme in this paper solves the problem of PCO nodes of different scales being in a congested state affecting the links between STA nodes and CCO nodes. The use of the mean shift algorithm does not require predetermination of the number of PCO nodes, thus allowing adaptive identification of the PCO nodes and access to the STA nodes corresponding to the PCO nodes. Alternate path creation can forward traffic from an uncongested PCO node to a CCO node when a small-scale PCO node is in a congested state. The PCO node election mechanism balances the available transmit bandwidth and buffer occupancy. It elects PCO nodes with larger available bandwidth and smaller buffer occupancy.

The simulation results from Figure 7 to Figure 9 show that the PCO node election mechanism achieves the best performance both in small-scale PCO nodes in a congested state and in large-scale PCO nodes in a congested state. The simulation results from Figure 10 to Figure 24 show that the proposed scheme has the best performance in terms of delay, packet loss rate, and throughput compared to the LEACH algorithm, the DCBSRP algorithm, Dijkstra's algorithm, and the SEAR algorithm for different numbers of packets sent by the STA nodes, different congested node available bandwidths, different congestion buffer occupancies, different buffer capacities, and different network scales. The Dijkstra algorithm transmits electricity consumption information directly according to the shortest hop path that is affected by congestion, and therefore has the worst performance. Although the SEAR algorithm can restore the communication capability of the link affected by congestion to a certain extent, the degradation of link quality caused by congestion is still more serious. Therefore, the SEAR algorithm is better than the Dijkstra algorithm in terms of performance. The LEACH algorithm selects PCO nodes more randomly. although the DCBSRP algorithm selects PCO nodes with smaller buffer occupancy, it neglects to filter the available transmit bandwidth. As a result, the selected PCO nodes often have poor available transmit bandwidth, and the network performance is worse than the LEACH algorithm. The proposed algorithm balances the available sending bandwidth and the buffer occupancy, and therefore achieves the best performance.

8. Conclusions

In this paper, a complete routing scheme is designed for dual-mode communication in the power Internet of Things to deal with the challenge of network congestion. The improved mean shift algorithm is used to determine the PCO nodes and the STA nodes accessing the corresponding PCO nodes without pre-setting the number of PCO nodes. The load balancing routing algorithm is presented for dual-mode communication networks based on alternate routing and PCO node election. Establishing alternate paths between PCO nodes and STA nodes can guarantee the transmission of electricity consumption information when small-scale PCO nodes are in a congested state. The PCO node election mechanism ensures link reliability when large-scale PCO nodes are in congestion.

The simulation results show that when the scale of PCO nodes in a congested state is small, the alternate path transfers the traffic in congested areas to non-congested areas. Meanwhile, the simulation results show that the PCO node election mechanism can be used in the phase of re-networking to elect PCO nodes with low buffer occupancy and high transmit available bandwidth to replace the PCO nodes in a congested state. In the future, an investigation is intended to ensure better performance of the communication link between STA nodes and CCO nodes when malicious nodes are present in the network.

Author Contributions: Methodology, Y.Y.; software, Z.L.; formal analysis, H.D. and K.X.; writing—original draft, Y.Y.; writing—review and editing, X.W. and Z.F.; project administration, J.C. and Z.F. All authors have read and agreed to the published version of the manuscript.

Funding: This work was supported by the State Grid Corporation of China with Grant No. 5700-202341281A-1-1-ZN, and the Natural Science Foundation on Frontier Leading Technology Basic Research Project of Jiangsu under Grant BK20212001.

Data Availability Statement: Data is contained within the article.

Conflicts of Interest: The authors declare no conflict of interest.

Abbreviations

The following abbreviations are used in this manuscript:

HPLC	High-speed Power Line Carrier
HRF	High-speed Radio Frequency
PCO	Proxy COordinator
CCO	Central COordinator
STA	Station
LEACH	Low Energy Adaptive Clustering Hierarchy
CH	Cluster Head
DCBSRP	Dynamic Cluster-Based Static Routing Protocol
SEAR	Simplified Energy-balanced Alternative-aware Routing

Appendix A

Appendix A.1

Algorithm A1 Mean Shift Algorithm

Input: $radius$,$data\_son\_node$

$m \leftarrow length(data\_son\_node)$
$index \leftarrow 1 : m$
while $isempty(index) == 0$ **do**
  $center \leftarrow data\_son\_node(index(ceil(length(index) \cdot rand)))$
  while $TRUE$ **do**
    $dis \leftarrow sum\left((repmat(center, m, 1) - data\_son\_node)^2, 2\right)$
    $innerS \leftarrow find\left(dis < radius^2\right)$
    $visitflag(innerS) \leftarrow 1$
    $this\_class(innerS) \leftarrow this\_class(innerS) + 1$
    for $i = 1 : length(innerS)$ **do**
      $w_i = \frac{e^{(dis(innerS(i)))}}{radius \cdot radius}$
      $sumweight \leftarrow w_i + sumweight$
      $center^{(l+1)} \leftarrow center^{(l)} + w_i \cdot data\_son\_node(innerS(i), :)$
    end for
    $center^{(l+1)} \leftarrow \frac{center^{(l+1)}}{sumweight}$
    if $norm\left(center^{(l+1)} - center^{(l)}\right) < stopthresh$ **then**
      break
    end if
  end while
  for $i = 1 : clustern$ **do**
    $betw \leftarrow norm(center - clustercenter(i, :))$
    if $betw < \frac{radius}{2}$ **then**
      $mergewith \leftarrow i$
      break
    end if
  end for
  if $mergewith == 0$ **then**
    $clustern \leftarrow clustern + 1$
    $clustercenter(clustern, :) = center^{(l+1)}$
    $count(:, clustern) \leftarrow this\_class$
  else
    $clustercenter(mergewith, :) = \frac{clustercenter(mergewith,:) + center^{(l+1)}}{2}$
    $count(:, mergewith) \leftarrow count(:, mergewith) + this\_class$
  end if
  $index \leftarrow find(visitflag == 0)$
end while
for $i = 1 : m$ **do**
  $Idx(i) \leftarrow \max(count(i, :))$
end for

Output: $clustern$,$clustercenter$,Idx

Algorithm A2 Shortest Hop Path Algorithm

Input: $total\_number, total\_link\_hop\_hrf, s, d$

for $i \leftarrow 1 : nodes\_number$ **do**
  $temp \leftarrow []$
  for $h \leftarrow 1 : nodes\_number$ **do**
    if $visited(h) == 0$ **then**
      $temp \leftarrow [temp\ distance(h)]$
    else
      $temp \leftarrow [temp\ inf]$
    end if
  end for
end for
if $parent(d) \neq 0$ **then**
  $t \leftarrow d$
  $path \leftarrow [d]$
  while $t \neq s$ **do**
    $p \leftarrow parent(t)$
    $path \leftarrow [\ p \quad path\ ]$
    $t \leftarrow p$
  end while
end if
$hop \leftarrow distance(d)$

Output: $path, hop$

References

1. Zou, J.; Yuan, Z.; Xin, P.; Xiao, Z.; Sun, J.; Zhuang, S.; Guo, Z.; Fu, J.; Liu, Y. Privacy-Friendly Task Offloading for Smart Grid in 6G Satellite–Terrestrial Edge Computing Networks. *Electronics* **2023**, *12*, 3484. [CrossRef]
2. Kim, M.; Shon, T. Digital Forensics for E-IoT Devices in Smart Cities. *Electronics* **2023**, *12*, 3233. [CrossRef]
3. Yu, Q.; Wang, X.; Lv, D.; Qi, B.; Wei, Y.; Liu, L.; Zhang, P.; Zhu, W.; Zhang, W. Data Fusion and Situation Awareness for Smart Grid and Power Communication Network Based on Tensor Computing and Deep Reinforcement Learning. *Electronics* **2023**, *12*, 2606. [CrossRef]
4. Fang, X.; Misra, S.; Xue, G.; Yang, D. Smart Grid—The New and Improved Power Grid: A Survey. *IEEE Commun. Surveys Tuts.* **2012**, *14*, 944–980. [CrossRef]
5. Galli, S.; Banwell, T.C. Modeling the indoor power line channel: New results and modern design considerations. In Proceedings of the First IEEE Consumer Communications and Networking Conference, Las Vegas, NV, USA, 5–8 January 2004; pp. 25–30.
6. Ma, H.; Lampe, L.; Hranilovic, S. Hybrid visible light and power line communication for indoor multiuser downlink. *IEEE J. Opt. Commun. Netw.* **2017**, *9*, 635–647. [CrossRef]
7. Hao, Y.; Zhou, C.; Zhang, X.; Zhao, D.; Li, F.; Wang, H. Power line communication challenges in the energy internet. In Proceedings of the International Conference on Smart Grid and Energy Engineering, Guilin, China, 13–15 November 2020; pp. 645–653
8. Natalizio, E.; Cavalcanti, D.; Chowdhury, K.; El Said, M. Advances in wireless communication and networking for cooperating autonomous systems. *Ad. Hoc. Netw.* **2018**, *68*, 13–18. [CrossRef]
9. Ye, F.; Sun, J.; Zhao, L.; Jiang, C.; Wang, C. An Adaptive Communication Routing Algorithm in Dual-mode Heterogeneous Field Network of Power Distribution Grid Based on RPL Protocol. In Proceedings of the 2022 9th International Forum on Electrical Engineering and Automation (IFEEA), Zhuhai, China, 4–6 November 2022; pp. 1084–1090.
10. Deng, F.; Yue, X.; Fan, X.; Guan, S.; Xu, Y.; Chen, J. Multisource energy harvesting system for a wireless sensor network node in the field environment. *IEEE Internet Things J.* **2019**, *6*, 918–927. [CrossRef]
11. Casella, I.R.S.; Anpalagan, A. Power line communication systems for smart grids. *Inst. Eng. Technol.* **2018**, *132*, 252–260.
12. Prajwal, K.S.; Amitasree, P.; Vamshi, G.R.; Kirthika Devi, V.S. Wireless communication network-based smart grid system. In *Pervasive Computing and Social Networking*; Springer: Singapore, 2022; Volume 317, pp. 673–694.
13. Noura, H.N.; Melki, R.; Chehab, A.; Fernandez, J.H. Efficient and robust data availability solution for hybrid PLC/RF systems. *Comput. Netw.* **2021**, *185*, 107675–107681. [CrossRef]
14. Taleb, T.; Jamalipour, A.; Kato, N.; Nemoto, Y. IP traffic load distribution in NGEO broadband satellite networks. In Proceedings of the Computer and Information Sciences-ISCIS 2005: 20th International Symposium, Istanbul, Turkey, 26–28 October 2005; pp. 113–123.
15. Zhou, C.; Hao, Y.; Zhang, X.; Li, Z.; Tang, X. Research on Low Power Design Technology of HPLC. *J. Phys. Conf. Ser.* **2021**, *1920*, 012050. [CrossRef]

16. Heinzelman, W.R.; Chandrakasan, A.; Balakrishnan, H. Energy- efficient communication protocol for wireless microsensor networks. In Proceedings of the 33rd Annual Hawaii International Conference on System Sciences, Maui, HI, USA, 7 January 2000; Volume 2, p. 10.
17. Chatterjee, M.; Das, S.K.; Turgut, D. An on-demand weighted clus- tering algorithm (WCA) for ad hoc networks. lobecom '00-IEEE. In Proceedings of the Global Telecommunications Conference. Conference Record (Cat. No.00CH37137), San Francisco, CA, USA, 27 November–1 December 2020; Volume 3, pp. 1697–1701.
18. Behera, T.M.; Mohapatra, S.K.; Samal, U.C.; Khan, M.S.; Daneshmand, M.; Gandomi, A.H. Residual Energy-Based Cluster-Head Selection in WSNs for IoT Application. *IEEE Internet Things J.* **2019**, *6*, 5132–5139. [CrossRef]
19. Elshrkawey, M.; Elsherif, S.M.; Wahed, M.E. 'An enhancement approach for reducing the energy consumption in wireless sensor net- works. *J. King Saud Univ.-Comput. Inf. Sci.* **2018**, *30*, 259–267.
20. Bendjeddou, A.; Laoufi, H.; Boudjit, S. LEACH-S: Low energy adap tive clustering hierarchy for sensor network. In Proceedings of the 2018 International Symposium on Networks, Computers and Communications (ISNCC), Rome, Italy, 19–21 June 2018; pp. 1–6.
21. Adil, M.; Khan, R.; Ali, J.; Roh, B.-H.; Ta, Q.T.H.; Almaiah, M.A. An Energy Proficient Load Balancing Routing Scheme for Wireless Sensor Networks to Maximize Their Lifespan in an Operational Environment. *IEEE Access* **2020**, *8*, 163209–163224. [CrossRef]
22. Yan, J.-F.; Liu, Y.-L. Improved LEACH routing Protocol for large scale wireless sensor networks routing. In Proceedings of the 2011 International Conference on Electronics, Communications and Control (ICECC), Ningbo, China, 9–11 September 2011; pp. 3754–3757.
23. Ammar, A.B.; Dziri, A.; Terre, M.; Y oussef, H. Multi-hop LEACH based cross-layer design for large scale wireless sensor networks. In Proceedings of the 2016 International Wireless Communications and Mobile Computing Conference (IWCMC), Paphos, Cyprus, 5–9 September 2016; pp. 763–768.
24. Qiang, T.; Bingwen, W.; Zhicheng, D. MS-leach: A routing Proto- col combining multi-hop transmissions and single-hop transmissions. In Proceedings of the 2009 Pacific-Asia Conference on Circuits, Communications and Systems, Chengdu, China, 16–17 May 2009; pp. 107–110.
25. Yektaparast, A.; Nabavi, F.-H.; Sarmast, A. An improvement on LEACH Protocol (Cell-LEACH). In Proceedings of the 2012 14th International Conference on Advanced Communication Technology (ICACT), Pyeong Chang, Korea South, 19–22 February 2012; pp. 992–996.
26. Kodali, K.R.; Aravapalli, K.N. Multi-level LEACH Protocol model using NS-3. In Proceedings of the 2014 IEEE International Advance Computing Conference (IACC), Gurgaon, India, 21–22 February 2014; pp. 375–380.
27. Zhang, J.; Chen, J.; Xu, Z.; Liu, Y. LEACH-WM: Weighted and intra cluster multi-hop energy-efficient algorithm for wireless sensor networks. In Proceedings of the 2016 35th Chinese Control Conference (CCC), Chengdu, China, 27–29 July 2016; pp. 8325–8329.
28. Nayak, P.; Devulapalli, A. A fuzzy logic-based clustering algorithm for WSN to extend the network lifetime. *IEEE Sensors J.* **2016**, *16*, 137–144. [CrossRef]
29. Elsmany, E.F.A.; Omar, M.A.; Wan, T.-C.; Altahir, A.A. EESRA: Energy Efficient Scalable Routing Algorithm for Wireless Sensor Networks. *IEEE Access* **2019**, *7*, 96974–96983. [CrossRef]
30. Katiyar, V.; Chand, N.; Soni, S. Clustering algorithms for heteroge neous wireless sensor network: A survey. *Int. J. Appl. Eng. Res.* **2010**, *1*, 273–287.
31. Smaragdakis, G.; Matta, I.; Bestavros, A. *SEP: A Stable Election Protocol for Clustered Heterogeneous Wireless Sensor Networks*; Department of Computer Science, Boston University: Boston, MA, USA, 2004; pp. 1–11.
32. Qing, L.; Zhu, Q.; Wang, M. Design of a distributed energy-efficient clustering algorithm for heterogeneous wireless sensor networks. *Comput. Commun.* **2006**, *29*, 2230–2237. [CrossRef]
33. Kumar, D.; Aseri, T.C.; Patel, R. EEHC: Energy efficient heteroge neous clustered scheme for wireless sensor networks. *Comput. Commun.* **2009**, *32*, 662–667. [CrossRef]
34. Behera, T.M.; Mohapatra, S.K.; Samal, U.C.; Khan, M.S.; Daneshmand, M.; Gandomi, A.H. I-SEP: An Improved Routing Protocol for Heterogeneous WSN for IoT-Based Environmental Monitoring. *IEEE Internet Things J.* **2020**, *7*, 710–717. [CrossRef]
35. Adil, M.; Khan, R.; Adil, M.; Almaiah, M.A.; Binsawad, M.; Ali, J.; Al Saaidah, A.; Ta, Q.T.H. An Efficient Load Balancing Scheme of Energy Gauge Nodes to Maximize the Lifespan of Constraint Oriented Networks. *IEEE Access* **2020**, *8*, 148510–148527. [CrossRef]
36. Dijkstra, E.W. A note on two problems in connexion with graphs. In *Edsger Wybe Dijkstra: His Life, Work, and Legacy*; ACM: New York, NY, USA, 2022; pp. 287–290.
37. Taleb, T.; Mashimo, D.; Jamalipour, A.; Hashimoto, K.; Nemoto, Y.; Kato, N. Sat04-3: Elb: An explicit load balancing routing protocol for multi-hop ngeo satellite constellations. *IEEE Globecom* **2006**, *2006*, 1–5.
38. Taleb, T.; Mashimo, D.; Jamalipour, A.; Kato, N.; Nemoto, Y. Explicit load balancing tech- nique for ngeo satellite IP networks with on-board process- ing capabilities. *IEEE/ACM Trans. Netw.* **2009**, *17*, 281–293. [CrossRef]
39. Song, G.; Chao, M.; Yang, B.; Zheng, Y. Tlr: A traffic-light-based intelli gent routing strategy for ngeo satellite ip networks. *IEEE Trans. Wireless Commun.* **2014**, *13*, 3380–3393. [CrossRef]
40. Dong, C.; Xu, X.; Liu, A.; Liang, X. Load balancing routing algorithm based on extended link states in LEO constellation network. *China Commun.* **2022**, *19*, 247–260. [CrossRef]

41. Mu, J.; Liu, X.; Yi, X. Simplified Energy-Balanced Alternative-Aware Routing Algorithm for Wireless Body Area Networks. *IEEE Access* **2019**, *7*, 108295–108303. [CrossRef]
42. Comaniciu, D.; Meer, P. Mean shift: A robust approach toward feature space analysis. *IEEE Trans. Pattern Anal. Mach. Intell.* **2002**, *24*, 603–619. [CrossRef]
43. Zhu, B.; Bedeer, E.; Nguyen, H.H.; Barton, R.; Henry, J. Improved Soft-k-Means Clustering Algorithm for Balancing Energy Consumption in Wireless Sensor Networks. *IEEE Internet Things J.* **2021**, *8*, 4868–4881. [CrossRef]
44. Hajian, E.; Khayyambashi, M.R.; Movahhedinia, N. A Mechanism for Load Balancing Routing and Virtualization Based on SDWSN for IoT Applications. *IEEE Access* **2022**, *10*, 37457–37476. [CrossRef]
45. Hassan, M.; Tariq, N.; Alsirhani, A.; Alsirhani, N.; Alomari, A.; Khan, F.A.; Alshahrani, M.M.; Ashraf, M.; Humayun, M. GITM: A GINI Index-Based Trust Mechanism to Mitigate and Isolate Sybil Attack in RPL-Enabled Smart Grid Advanced Metering Infrastructures. *IEEE Access* **2023**, *11*, 62697–62720. [CrossRef]
46. Wang, K.; Wu, J.; Zheng, X.; Li, J.; Yang, W.; Vasilakos, A.V. Cloud-Edge Orchestrated Power Dispatching for Smart Grid with Distributed Energy Resources. *IEEE Trans. Cloud Comput.* **2023**, *11*, 1194–1203. [CrossRef]